PASJ: Publ. Astron. Soc. Japan , 1–**??**,

Comparison of AGN and Nuclear Starburst Activity in Seyfert 1 and 2 Galaxies over a Wide Luminosity Range Based on Near-infrared 2–4 μm Spectroscopy

Nagisa OI[1,2,3]
nagisa.oi@nao.ac.jp
Masatoshi IMANISHI[2,1,3] & Keisuke IMASE[1,2]
[1]*Department of Astronomical Science, The Graduate University for Advanced Studies (Sokendai), Mitaka, Tokyo 181-8588, Japan*
[2]*National Astronomical Observatory of Japan, Mitaka, Tokyo 181-8588, Japan*
[3]*Present Address; Subaru Telescope, 650, North A'ohoku Place, Hilo, HI 96720, USA*

(Received ; accepted)

Abstract

We present near-infrared K- (1.9–2.5μm) and L- (2.8–4.2μm) band spectroscopy of 22 Seyfert nuclei. We use two methods to investigate the presence of nuclear starbursts: (1) the Polycyclic Aromatic Hydrocarbon (PAH) emission feature at λ_{rest} = 3.3 μm in the rest frame of L-band spectrum (a starburst indicator) and (2) the CO absorption feature at λ_{rest} = 2.3–2.4 μm in the rest frame of the K-band spectrum, originating in the CO molecule. We clearly detected the 3.3 μm PAH emission features in five objects and the CO absorption features in 17 objects. Seyfert 2 galaxies tend to show bluer $K-L$ colors compared with Seyfert 1 galaxies. We interpret the discrepancy as resulting from relative strength of stellar emission because AGN emission is affected by dust extinction. The 3.3 μm PAH emission luminosity ($L_{3.3PAH}$) distributions for the Seyfert 1s and Seyfert 2s are very similar when normalized to the AGN power. Star-formation rates estimated from $L_{3.3PAH}$ could be large enough to inflate the dusty torus by supernova explosion. We find that $L_{3.3PAH}$ positively correlates with N-band luminosity with small aperture over a wide AGN luminosity range, and is independent of physical area we probed. The results suggest that nuclear region has a concentration of star formation and the star formation would control AGN activity.

Key words: active — galaxies:nuclei — galaxies:Seyfert — galaxies:starburst — infrared:galaxies

1. Introduction

A galaxy that exhibits bright emission in the nuclear region is termed an Active Galactic Nucleus (AGN). The origin of the radiative energy is putative release of gravitational energy through accretion of the interstellar medium from the host galaxy onto a central super-massive black hole (SMBH) with a mass of $>10^6 M_\odot$. Starbursts are one of the candidates for transporting material onto the center (Wada & Norman 2002), so studying the correlation between AGNs and starbursts is crucial to understanding the origin of AGN activity. Seyfert galaxies are the second most numerous AGN class in the local universe[1]. They are classified into two types: type 1 Seyfert galaxies show broad and narrow optical emission lines, and type 2 Seyfert galaxies show narrow emission lines only. The difference is explained by the AGN unification paradigm (Antonucci 1993) in which molecular gas and dust with a torus-shaped structure (the so-called dusty torus) surrounds the central SMBH. The intrinsic AGN properties of the two types of Seyfert galaxies are assumed to be the identical. The dusty torus plays various roles in observed spectra: (1) obscures the AGN for a Seyfert 2 galaxy and (2) absorbs the energetic radiation from the AGN and re-radiates it as infrared dust emission for both types of Seyfert galaxies. Because the torus is composed of significant amounts of molecular gas and dust, it is a natural site for star formation. In particular, the outer portion of the torus is thought to be an ideal site for star formation because star formation can be suppressed in the inner portion by tidal forces from the SMBH. In fact, it was argued that such starburst activity could occur in the dusty torus in the nuclear region (<100pc) of a Seyfert galaxy (Wada & Norman 2002; Imanishi 2003). We call such starbursts in Seyfert nuclei "nuclear starbursts". Wada & Norman (2002) showed that the nuclear starbursts in the dusty torus can produce an inflated turbulent torus around the central SMBH. However, with limited spatial resolution, it is difficult to detect the emission from the nuclear starbursts as they are diluted by strong AGN emission. Here, we discern these emission and estimate the magnitudes of starburst activities using infrared K-band (1.9–2.5μm) and L-band (2.8–4.2μm) spectra.

Polycyclic Aromatic Hydrocarbon (PAH) emission at around 3.3 μm in the L-band is a powerful tool for distinguishing starburst emission from AGN emission. PAH molecules are widely distributed throughout interstellar space (Tanaka et al. 1996). The PAH molecules are not destroyed and are excited by non-ionizing UV photons from stars and then emit the line at 3.3 μm in the Photo-Dissociation Region (PDR) for starburst (Sellgren 1981), whereas the PAH molecules are destroyed by X-rays (Voit 1992) from AGN. Observationally, a normal starburst galaxy, which consists of HII regions, PDRs, and molecular gas (e.g. M82 and NGC253), shows the 3.3 μm PAH emission (Tokunaga et al. 1991; Imanishi & Dudley 2000),

[1] It assumes that LINERs are powered by AGN (Ho et al. 1997)

whereas a pure AGN shows only PAH-free continuum emission from larger-sized AGN-heated hot dust grains (Moorwood 1986; Imanishi & Dudley 2000) because an AGN emits strong X-rays in addition to UV. Additionally, because the 3.3 μm PAH emission feature is very strong, it is detectable even if the starbursts are weak.

Nuclear starbursts in Seyfert galaxies can also be investigated through infrared K-band spectra. The CO(Δv=2–0) absorption feature at λ_{rest}=2.3–2.4 μm is caused by the CO molecule in the photosphere of cool stellar population (i.e. red giants and supergiants) (Frogel et al. 1978; Doyon et al. 1994). Empirically, starburst galaxies exhibit a substantially deeper CO(Δv=2–0) feature than do quiescent spirals galaxies (Frogel et al. 1978; Ridgway et al. 1994), and AGNs do not exhibit this absorption feature.

Furthermore dust extinction is much lower in the K- and L-bands than at shorter wavelengths, $A_K \sim 0.062 A_V$ and $A_L \sim 0.031 A_V$, respectively (Nishiyama et al. 2008; Nishiyama et al. 2009), so that the quantitative uncertainty of the dust extinction correction is significantly reduced compared with shorter wavelengths (e.g. UV, optical). Thus, K- and L-band spectra enable us to estimate the relative contributions of AGN and starbursts emission to an observed spectrum in a quantitatively reliable manner (Oliva et al. 1999; Ivanov et al. 2000; Rodríguez-Ardila & Viegas 2003; Imanishi 2003; Imanishi & Alonso-Herrero 2004; Imanishi & Wada 2004; Davies et al. 2007).

The above authors studied mainly nearby Seyfert galaxies with high infrared luminosities ($L_{IR} \gtrsim 10^{44}$ergs s^{-1}), and found a correlation between the AGN activity and nuclear starburst activity (Imanishi 2003; Imanishi & Alonso-Herrero 2004; Imanishi & Wada 2004). However, it is unclear whether the correlation holds over a wide range of AGN luminosity. Haas et al. (2005) argued that the height of the torus is smaller in lower luminosity Seyfert galaxies compared with higher luminosity Seyfert galaxies, suggesting that nuclear starbursts are weaker in low-luminosity AGNs. In contrast, Ballantyne (2008) predicted that parsec-scale starbursts would be associated with lower luminosity AGNs. Kawakatu & Wada (2008) predicted that the ratio of the scatter in the AGN to starburst luminosity would increase in low-luminosity AGNs. To resolve this issue, it is necessary to study Seyfert galaxies over a wide AGN luminosity range. Thus, we performed K- and L-band spectroscopy of a large sample of Seyfert galaxies with luminosity ranging from low to high. Throughout the paper, $H_0 = 75$km s^{-1}Mpc^{-1}, Ω_M =0.3, Ω_Λ =0.7 are adopted.

2. Target Selection

Imanishi (2003), Imanishi & Alonso-Herrero (2004), and Imanishi & Wada (2004) studied Seyfert galaxies taken from the CfA (Huchra & Burg 1992) and 12 μm (Rush et al. 1993) samples. The CfA and 12 μm samples were selected through optical spectroscopy of large numbers of galaxies limited by optical and $IRAS$ 12 μm fluxes, respectively. The CfA sample is usually regarded as a complete sample of optically selected Seyfert galaxies. However, Ho & Ulvestad (2001) argued that the CfA sample is likely to be complete only for relatively bright objects.

Therefore we added objects from the Palomar sample (Ho et al. 1995) in this paper. Seyfert galaxies in the Palomar sample are selected through optical spectroscopy of nearby, bright ($B_T \leq$12.5 mag), northern (declination $>0^\circ$) galaxies covering a wider AGN luminosity range. Our aim is to confirm the relationship between AGN and nuclear starburst activity over a wide AGN luminosity range, paying particular attention to low-luminosity AGN. To be easily observable from Mauna Kea, Hawaii (our observing site; latitude $\sim$20°), the declinations of Seyfert galaxies were limited to greater than -30°. Owing to the telescope limit on the IRTF 3.0-m telescope used in this study, a restriction on declination of less than 68° was also applied. In total, 13 objects in the Palomar Sample (Table 1) were observed. We also added some additional re-observed Seyfert galaxies to our targets. These galaxies are those studied by Imanishi (2003), Imanishi & Alonso-Herrero (2004) and Imanishi & Wada (2004), in which PAH emission was barely discernible, but with less than 3σ, as reported in these papers (NGC262, NGC513, Mrk993, MCG–3-58-7, F03450+0055, NGC931 and NGC5548). Moreover, we also included 0152+06 in the CfA sample and MCG–2-8-39 in the 12 μm sample in our targets. Both of them meet the declination criteria of these paper but were not observed in previous papers. To summarize, 13 objects from the Palomar sample, seven re-observed objects discussed in previous papers, and two new objects from CfA and 12 μm samples are included in this paper.

Six of the 22 targets are Seyfert 1 galaxies and the remaining 16 targets are Seyfert 2 galaxies. Infrared (8-1000 μm) luminosity of our targets is logL_{IR}=42.5–44.8 ergs s^{-1} for the Palomar sample and logL_{IR}=43.6–44.8 ergs s^{-1} for the CfA and 12μm samples (see a caption of Table 1 for the definition of L_{IR}). Detailed information on the targets is summarized in Table 1. We define type 1–1.5 and type 1.8–2 Seyfert galaxies as Seyfert 1 and Seyfert 2 galaxies, respectively. Mrk993 was classified as a Seyfert 2 galaxy in the CfA sample, but later reclassified as a Seyfert 1.5 galaxy (Osterbrock & Martel 1993). We adopt the latter classification and thus classified it as a Seyfert 1 galaxy, although it was regarded as a Seyfert 2 galaxy by Imanishi & Alonso-Herrero (2004).

3. Observations & Data Analysis

Table 2 summarizes our observation log. All targets were observed with SpeX (Rayner et al. 2003) on the IRTF 3.0-m telescope on Mauna Kea, Hawaii. SpeX has a 1.9–4.2μm cross-dispersed spectroscopic mode (LXD1.9 mode), enabling us to observe K- and L-band spectra simultaneously. Because the seeing in K measured with the SpeX guiding/imaging mode was about 0.″4–0.″8 (FWHM) throughout the observations (except on 26 and 27 March 2009), we consistently used a 0.″8-wide slit. On 26 and 27 March 2009, the seeing was over 1.″0 at K, so we used a 1.″6-wide slit during those observations. A standard telescope nodding technique (ABBA pattern) with a throw of 7.″5 was employed along the slit to subtract background emission. The physical scale probed by our slit spectroscopy is 24–500 pc taking into account the redshift, z = 0.002–0.032, and slit width. We observed A-, F- and G-type main-sequence stars (Table 2) as standard stars. These

were used to correct for transmission through the Earth's atmosphere. We observed the standard stars at airmasses similar to the targets (<0.1 difference), before and after the observation of each target to better correct for possible time variations in the Earth atmosphere.

The spectra were reduced using standard IRAF tasks.[2] Frames taken with an A (B) beam were subtracted from frames taken with a B (A) beam, and then median images were taken and divided by a spectroscopic flat image. Known bad pixels and remaining pixels hit by cosmic rays were replaced with interpolated values from the surrounding pixels. The Seyfert galaxies and standard-star spectra were then extracted by integrating signals over 1.″3–2.″5 along the slit. The one-dimensional spectrum was extracted by fitting the signals in each spectral order in the two-dimensional image. We used the wavelength-dependent nature of transmission through the Earth's atmosphere for our wavelength calibration. The object spectra were divided by spectra of standard stars to remove the effects of atmospheric absorption and then multiplied by the spectra of blackbodies with temperatures corresponding to those of the individual standard stars (Table 2). Flux calibration was performed based on the signal detected inside our slit, taking into account the differences in exposure time between our targets and the standard stars. K- and L-band magnitudes for the standard stars were estimated from their V-band magnitudes, adopting appropriate $V-K$ and $K-L$ colors for each individual standard star stellar type (Tokunaga 2000). A strong methane absorption line appears λ_{rest} = 3.315μm in the Earth's atmosphere. Although this could be corrected by standard stars in theory, it introduces a relatively strong amount of noise. Thus, we excluded a few data points at around λ_{rest} = 3.315 μm, whose transmission were less than 40% of nearby signals without being affected by the absorption line.

4. Results

4.1. L-band spectrum

Figure 1 shows flux-calibrated 3.0–3.6 μm slit spectra in the L-band. Although the full L-band (2.8–4.2 μm) wavelength range is covered by SpeX, both ends of the L-band are noisy because of poor transmission through the Earth's atmosphere ($\lambda < 3.0\mu$m) and high background emission from the Earth's atmosphere ($\lambda > 3.6\mu$m). We removed those data points for the discussions in this paper because they were not necessary for our scientific aims. In these plots, some objects show a clear excess at 3.29 μm$\times$(1+z) whose wavelength corresponds to the redshifted 3.3 μm PAH emission feature. We regard the features as detected when at least two consecutive data points at around 3.29 μm$\times$(1+z) are higher than 1.5 times the scatter of the continuum level. Using this criterion, objects with detectable PAH emission are marked with "3.3 μm PAH", and PAH non-detected objects are marked with "3.3 μm PAH(?)" in the figure. We fitted the emission line to a Gaussian function by setting the normalization, full width of half maximum (FWHM) and central wavelength of the emission as free parameters, and then estimated the flux ($f_{3.3PAH}$), luminosity ($L_{3.3PAH}$) and rest-frame equivalent width ($EW_{3.3PAH}$) of the 3.3 μm PAH emission. For objects with no clear PAH emission features, we estimated upper limits by fitting the emission line with a Gaussian function whose height, central wavelength and FWHM were fixed as 3 σ, where 1 σ was a dispersion of its continuum emission, 3.29$\times$(1+z)μm and 0.02$\times$(1+z)μm (Tokunaga et al. 1991), respectively. The strengths of the 3.3 μm PAH emission features are summarized in Table 3.

The 3.3 μm PAH emission feature is detected in $\sim$ 23% (5/22) of the observed Seyfert galaxies (NGC6764, 5194, 5273, F03450+0055 and MCG-3-58-7). NGC6764 shows a strong PAH emission feature, and its rest-frame equivalent width ($EW_{3.3PAH}$) is as high as those of starburst galaxies ($\sim$100 nm; Imanishi & Dudley 2000). Although four objects (NGC5194, NGC5273, F03450+0055 and MCG-3-58-7) show detectable 3.3 μm PAH emission, the $EW_{3.3PAH}$ values are significantly smaller than $\sim$100 nm. The other 17 objects do not display detectable PAH features.

4.2. K-band spectrum

Flux-calibrated 2.0–2.5 μm slit spectra in the K-band are shown in Figure 2. Most of the spectra show a flux depression at $\lambda_{obs} > 2.3\mu$m in the observed frame, which is attributed to the CO (Δv=2–0) molecular absorption feature. The strength of the CO absorption feature was quantified by a spectroscopic CO_{spec} index defined by Doyon et al. (1994) as follows:

$$CO_{spec} \equiv -2.5 log_{10} \langle R_{2.36} \rangle,$$

where $\langle R_{2.36} \rangle$ is an average of actual signal at λ_{rest} = 2.31–2.40 μm divided by a power-law continuum ($F_\lambda = \alpha \times \lambda^\beta$) extrapolated from shorter wavelengths. As some strong emission features appear at around 2μm in K-band, such as H_2 1–0 S(1) ($\lambda_{rest} = 2.122\mu$m), Br$\gamma$ ($\lambda_{rest} = 2.166\mu$m) and H_2 1–0 S(0) ($\lambda_{rest} = 2.223\mu$m), we used data points at $\lambda_{rest} = 2.1 - 2.29\mu$m to fit the continuum level after excluding these emission lines. The continuum level is shown as a solid line in Figure 2. The CO_{spec} of all our targets are given in Table 3. The CO_{spec} values of cool stars are typically 0.2–0.3 (Doyon et al. 1994). For objects with a clear CO absorption feature ($CO_{spec} > 0.02$), "CO absorption" signature is written in Figure 2. About 77 % (17/22) of observed Seyfert galaxies show clear CO absorption features. Figure 3 is a histogram of the CO_{spec} of Luminous Infrared Galaxies (LIRGs: their luminosities are generally explained by starbursts) measured by Ridgway et al. (1994). It suggests that their typical value is also $\sim$ 0.2–0.3. If the properties of nuclear starbursts in Seyfert galaxies are similar to those of starbursts in LIRGs, the CO_{spec} of the starbursts in Seyfert galaxies is also expected to be 0.2–0.3. However, the observed CO_{spec} is smaller than the typical value for a LIRG because featureless AGN emission is superposed in the K-band spectrum.

[2] IRAF is distributed by the National Optical Astronomy Observatories, operated by the Association of Univers ities for Research in Astronomy (AURA), Inc., under cooperative agreement with the N ational Science Foundation.

5. Discussion

5.1. $K-L$ color

Because we took K- and L-band spectra simultaneously, possible slit loss caused by IRTF/SpeX tracking error is similar and sky conditions are the same for the K- and L-bands. Therefore, the derived $K-L$ colors are very reliable. The emission from normal stars (>2000K) in the L-band is much weaker than in the K-band, whereas hot (∼1000K) dust heated by an AGN emits strongly in both the K- and L-bands. Thus the $K-L$ colors become smaller (bluer) with increasing relative contribution from stellar emission to the total emission of nuclear region. Indeed, intrinsic $K-L$ colors of Seyfert 1 galaxies are typically 1–2 mag (Alonso-Herrero et al. 2003)[3], and those of normal spiral galaxies are $K-L<0.4$ (Willner et al. 1984). Therefore, the color enables us to distinguish starburst-important Seyfert galaxies from AGN-dominant ones. The nuclear $K-L$ colors derived from our slit spectra are summarized in column (6) of Table 3.

For the combined sample used in this paper, taken from Imanishi (2003), Imanishi & Alonso-Herrero (2004) and Imanishi & Wada (2004), we compared the $K-L$ colors of Seyfert 1 and 2 galaxies (Figure 4). Most of the Seyfert 1 galaxies are distributed in the $K-L=$ 1–2 mag range, whereas the colors of almost half of Seyfert 2 galaxies are bluer than the Seyfert 1 galaxies ($K-L<1$ mag). It shows that stellar contamination is relatively larger in Seyfert 2s than Seyfert 1s in the observed total emission. Two possibilities could explain the result. First, AGN emission is strongly affected by the extinction of dusty torus compared with nuclear starburst emission. In the AGN unified model, as the AGN emission comes from the central region, the emission from a Seyfert 2 galaxy passes through the dusty torus and is more strongly absorbed by the dusty torus than those from a Seyfert 1 galaxy. So, observed AGN emission of Seyfert 2 galaxies would be relatively weak in comparison to Seyfert 1 galaxies. Whereas, if the nuclear starbursts are occurring in the outer region of the dusty torus, then the absorption effect would not be much difference between these types of Seyfert galaxies. In this case, the starburst contribution to the total emission would be relatively significant in Seyfert 2s when compared with Seyfert 1s and then the $K-L$ colors of Seyfert 2s would be bluer than those of Seyfert 1s. Another possible explanation is the starbursts in the central region in Seyfert 2 galaxies could be more active than those in Seyfert 1 galaxies. If strong nuclear starbursts inflate the dusty torus more thickly than weaker starbursts, then a Seyfert galaxy with active starbursts is much more likely to be observed as type 2, and the color of it would be bluer than one with weak starbursts. However, as we will discuss in §6.0.1, we find no clear difference between Seyfert 1 and 2 galaxies in quantitatively measured 3.3 μm PAH luminosity. So, it is unlikely that the difference of the $K-L$ colors between Seyfert 1s and 2s is caused by the intrinsic difference of starburst activities in them. Therefore we suggest that the bluer $K-L$ colors of Seyfert 2s than Seyfert 1s are due to the obscuration of AGN emission and to relative contamination of the stellar emission in Seyfert 2 galaxies. Kotilainen et al. (1992) and Alonso-Herrero et al. (1996) deconvolved surface brightness profile of Seyfert 1s and 2s within 3-arcsec aperture into a combination of a nuclear source (non-stellar component), a bulge component and a disk component, and suggested that the stellar contamination to the total emission is larger in Seyfert 2s than in Seyfert 1s.

Figures 5a and 5b show the $K-L$ color versus the $EW_{3.3PAH}$ and CO_{spec} of the sample. These figures show that both the $EW_{3.3PAH}$ and CO_{spec} decrease with reddening $K-L$ color. Thus they are useful tracers for estimating the starburst contribution to the nuclear spectra inside our slit. The trends of Seyfert 2 galaxies in Figure 5 are similar to those for Seyfert 1 galaxies. In Figure 5b, however, some fraction of Seyfert 2 galaxies in our sample reach to CO_{spec} = 0.2–0.3, which is closer to those of LIRGs, in comparison to Seyfert 1 galaxies. This is good agreement with the suggestion above. In other words, the CO_{spec} of some fraction of Seyfert 2 galaxies are not strongly diluted by AGN emission.

6. Comparison of nuclear starbursts with AGN power

6.0.1. $IRAS$ 12 and 25 μm luminosity

We compare the nuclear starburst activity with AGN activity over a wide AGN luminosity range. The nuclear starburst activity is reasonably quantifiable from the observed 3.3 μm PAH emission luminosity inside our slit spectrum. Meanwhile Alonso-Herrero et al. (2003) showed that the obscuring effects of the AGN emission for Seyfert galaxies became insignificant at longer than 10 μm. $IRAS$ 60 and 100 μm luminosities contain more contamination of emission from star formation in the host galaxy than do $IRAS$ 12 and 25 μm luminosities (Spinoglio & Malkan 1989; Rodriguez Espinosa & Perez Garcia 1997; Alonso-Herrero et al. 2002), so we use $IRAS$ 12 and 25 μm luminos ities as good tracers of AGN power in Seyfert galaxies. A comparison between the $IRAS$ 12 and 25 μm luminosities and the observed nuclear 3.3 μm PAH emission luminosity is shown in Figures 6a and 6b, respectively. In these figures, we combined with the data of four sources observed by Rodríguez-Ardila & Viegas (2003) using the 0.″8 slit width of IRTF/SpeX.

We see no clear difference in the $L_{3.3PAH}$ between the two types of Seyfert galaxies when normalized to the AGN power. This means that we see no evidence of the possibility that Seyfert 2 galaxies tend to show intrinsically stronger starburst activities than do Seyfert 1 galaxies, a possibility discussed in §5.1. In Figure 6, the nuclear 3.3 μm PAH luminosities for our objects combined with previous data are $L_{3.3PAH}\sim10^{38}$–10^{42} ergs s^{-1} . In starburst-dominated galaxies, the 3.3 μm PAH-to-far-infrared (40–500 μm) luminosity ratios ($L_{3.3PAH}/L_{FIR}$) are $\sim1\times10^{-3}$ (Mouri et al. 1990). The nuclear star-formation rates (SFR) are calculated by SFR M$_\odot$ yr^{-1} = ($L_{\rm FIR}/2.2\times10^{43}$ ergs s^{-1}) (Kennicutt 1998). So the SFR of our sample could be up to 4.5–450$\times10^{-3}$M$_\odot$ yr^{-1}. Wada et al. (2009) showed that a supernova rate (SNR) of 5.4 to 540 $\times10^{-5}$ yr^{-1}, corresponding to 7.7–770$\times10^{-3}$M$_\odot$ yr^{-1} (SNR $\simeq$ 0.007 SFR), can produce torus heights of as large as 10 pc at the outer side $\simeq$ 5 pc. Hence, the star-formation rate of

[3] K′ was used in Alonso-Herrero et al. 2003; we assumed the differ ence between K′ and K was negligible.

almost our entire sample could be high enough to create a geometrically thick dusty torus. We should note, however, that we have only upper limits on the nuclear 3.3 μm PAH luminosities for many objects in our sample, so it is likely that the sample contains Seyfert galaxies that do not have a thick dusty torus.

The figures show that the nuclear starburst luminosity decreases with decreasing AGN power and that the trend dose not change over a wide AGN luminosity range. The ratios of starburst activity to AGN activities for both Seyfert 1 and 2 galaxies show the same levels of scatter and we find no obvious difference between them. We apply the generalized Kendall rank correlation statistics provided in the Astronomy Survival Analysis package (ASURV: Isobe et al. 1986) (which handles data with upper limits) to Figures 6a and 6b. The probabilities that a correlation is not present for the figures are both found to be $\sim$0.00%. The results show that there are tight correlation between 3.3 μm PAH luminosity in central region and $IRAS$ 12 and 25 μm luminosities.

6.0.2. Ground-based N-band luminosity

Although the contamination from star formation activity in $IRAS$ 12 and 25 μm is less than in the $IRAS$ 60 and 100 μm, it could be that the $IRAS$ 12 and 25 μm data still contain a significant amount of emission from star-forming activity of host galaxies in our low luminosity AGN sample, given the large aperture of $IRAS$ 12 μm ($0\farcm75 \times 4\farcm5$) and 25 μm ($0\farcm75 \times 4\farcm6$). Ramos Almeida et al. (2009) compared small aperture unresolved nuclear 10 μm emission ($0\farcs4$–$0\farcs5$) and 20 μm emission ($0\farcs5$–$0\farcs6$) with the $IRAS$ 12 μm and 25 μm emission, respectively, and found the large aperture data are largely contaminated by starlight. So it is likely that the $IRAS$ 12 μm and 25 μm emission is significantly contaminated by star formation in host galaxies. To reduce the possible ambiguity, we should compare the 3.3 μm PAH emission with an AGN indicator measured with a smaller aperture. The N-band (λ_0=10.78μm, $\Delta\lambda$=5.7μm) is observable from the ground, and its luminosity is also thought to be a good tracer of AGN power (Alonso-Herrero et al. 2002; Ramos Almeida et al. 2009; Levenson et al. 2009). Gorjian et al. (2004) presented N-band photometric data for the central regions of Seyfert galaxies. They used the Palomar 5-m telescope with a $1\farcs5$ aperture. Only 41% (9/22) of our objects were measured by Gorjian et al. (2004). We combine these with data from Imanishi & Wada (2004), which is shown in Figure 7. Although the number of low-luminosity AGNs is small and their 3.3 μm PAH emission luminosities are only upper limits, the three low luminosity Seyfert galaxies are distributed around a line extrapolated from the stronger AGN activity region. We also apply the generalized Kendall rank correlation statistics to Figure 7. The uncorrelated probability is $\sim$0.03% for the figure. These results mean that the correlation between the luminosities of the nuclear starbursts detected inside the slit spectra and central AGNs is statistically confirmed in Seyfert galaxies for all observed quantities.

We found the relation between the luminosities of 3.3 μm PAH emission within our slit width and of N-band. However it is worried that the $L_{3.3PAH}$ is affected by physical aperture size probed by the slits. It means that we are concerned about the possibility that the $L_{3.3PAH}$ of the most luminous object is due to the largest area we observed. If star formation traced by $L_{3.3PAH}$ is spatially extending in a wide area of host galaxy, then the $L_{3.3PAH}$ becomes higher with lager physical scale. To explore this, we compare the $L_{3.3PAH}$ with physical area of each source (Figure 8). The figure clearly shows that not all high $L_{3.3PAH}$ objects are wide physical area coverage. That is to say, the star formation would be occurring in the central region inside the slits and not spatially extend.

6.1. Trigger of accretion onto SMBH

We find no evidence that the ratio of starbursts to AGN luminosity deviates upward in low-luminosity AGNs, as predicted by Kawakatu & Wada (2008), or that nuclear starburst activities increase with decreasing AGN activities as predicted by Ballantyne (2008). Furthermore, we find no clear change in the correlations over a wide AGN luminosity range. This is explained if the main mechanism that connects the AGN and nuclear starbursts is the same at each luminosity range. A model shown in Wada & Norman (2002; see also Wada et al. 2009), which predicts the enhancement of a mass accretion rate onto a central SMBH owing to increased turbulence of molecular gas in the torus caused by nuclear starbursts, is one possible scenario that could account for the luminosity correlation.

6.2. The origin of the CO_{spec} index

We calculated stellar luminosity ($L_{Kstellar}$) from CO_{spec}. If nuclear starbursts with properties similar to star-formation-dominated LIRGs appear inside our slit and the entire K-band emission comes from stars, then the detected CO_{spec} must be 0.2–0.3. We assumed the original CO_{spec} of the cool star was 0.25. When the contributions of stellar emission to total emission are 100%, the average signal at λ_{rest} = 2.31–2.4μm is reduced by about 20.5% compared with an extrapolation from a shorter wavelength. When the contribution of AGN emission to the total emission is 100 %, the absorption feature does not appear. When the contributions of both stellar and AGN emission are equal, the average signal at λ_{rest} = 2.31–2.4μm should be 10.25% reduced from the shorter wavelength, and the CO_{spec} should be 0.117. In the case that the CO_{spec} is 0.1 or 0.15, the contributions of stellar emission to total emission should be 43% or 63%, respectively. So, we can estimate the $L_{Kstellar}$. Figure 9 compares the $L_{Kstellar}$ and the 3.3 μm PAH emission luminosity in the nuclear region detected inside our slit spectra combined with Fig. 5 of Imanishi & Alonso-Herrero (2004). Although they plotted these results for Seyfert 2 galaxies only, we included in Figure 9 Seyfert 1 galaxies whose CO_{spec} were derived in Imanishi & Wada (2004).

The K-band to infrared luminosity ratios of starburst-dominated LIRGs were estimated to be $L_K/L_{IR(8-1000\mu\mathrm{m})} \sim 10^{-1.6\pm0.2}$ (Goldader et al. 1997). If the nuclear starbursts in Seyfert galaxies have properties similar to the starburst-dominated LIRGs, then the same relation should hold. The 3.3 μm PAH to infrared luminosity ratios in starbursts were found to be $L_{3.3PAH}/L_{FIR(40-500\mu\mathrm{m})} \sim 10^{-3}$ (Mouri et al. 1990). Assuming $L_{IR} \sim L_{FIR}$ for starbursts, the luminosity of the 3.3 μm PAH emission to the K-band stellar luminosity ratios are expected to be $L_{3.3PAH}/L_{Kstellar} \sim 10^{-1.4}$, if both luminosities trace the same starbursts. The value is shown as a solid line in Figure 9. Most of our Seyfert 1 galaxies and about half of the Seyfert 2 galaxies plotted in the figure are distributed around the line. However, the remaining half of the

Seyfert 2 galaxies are distributed under the line. Given that in Figure 6, the $L_{3.3PAH}$ distribution of both Seyfert 1 and 2 galaxies is similar within their dispersions and no obvious difference is seen between them, the discrepancy must be caused by $L_{Kstellar}$. As we discussed above, the $L_{Kstellar}$ is estimated from the CO_{spec} value, which is related to the fraction of stellar to AGN emission. Nuclear starbursts are expected to occur at the outer part of the dusty torus and the AGN radiation of type 2 Seyfert galaxy is significantly attenuated by the dusty torus. Therefore, the CO_{spec} is likely to increase and thus increase $L_{Kstellar}$ in Seyfert 2 galaxies. In contrast, because $L_{3.3PAH}$ is estimated from the flux of 3.3 μm PAH emission, PAH-estimated starburst luminosity is not affected by the absorption of AGN emission. In summary, we suggest that because $L_{Kstellar}$ represents a relative value of stellar to AGN emission and $L_{3.3PAH}$ represents an absolute value of stellar emission, it is possible that $L_{Kstellar}$ is overluminous and that the ratio of $L_{3.3PAH}/L_{Kstellar}$ decreases in Seyfert 2 galaxies.

The other possibility is that the signatures of stellar emission detected in the K-band spectra are significantly contaminated by old bulge stars in the nuclear part of the host galaxy, whereas the 3.3 μm PAH emission originates in spatially unresolved (smaller than subarcsecond) nuclear starbursts in the dusty torus because old stars do not have enough PAH-exciting UV photons. Ivanov et al. (2000) and Imanishi & Alonso-Herrero (2004) suggested that the emission of old stars in the host galaxy mainly produces the K-band spectra. However, most of the Seyfert 1 and some fraction of the Seyfert 2 galaxies have $L_{3.3PAH}/L_{Kstellar}$ ratios similar to the value expected when the origin of both luminosities is the same. Therefore, although the old stars in host galaxy may contribute to the observed K-band spectra of some fraction of Seyfert galaxies, it is not likely that old stars dominate the K-band spectra in all objects.

7. Conclusion

The results of an infrared K- and L-band spectroscopic study of 13 Seyfert galaxies from the Palomar sample, and seven Seyfert galaxies with non-detectable 3.3 μm PAH emission discussed in previous papers and two new Seyfert galaxies from CfA and 12μm samples are presented. Our L-band spectroscopic method successfully detected the 3.3 μm PAH emission in $\sim$ 23 % (=5/22) of the observed Seyfert galaxies. Also, our K-band spectroscopic method showed $\sim$ 77 % (=17/22) of Seyfert nuclei in our sample have clear CO absorption feature. We examined the relationship between AGN activity and nuclear starburst activity over a wide AGN luminosity range using our spectra together on previously published spectra (Imanishi 2003; Imanishi & Alonso-Herrero 2004; Imanishi & Wada 2004). Our conclusions are summarized as follows:

1. The $K-L$ colors of Seyfert 2 galaxies are widely distributed toward the blue, compared with those of Seyfert 1 galaxies. This implies either that the dusty torus absorbs the AGN emission of Seyfert 2 galaxies from the central region or that Seyfert 2 galaxies tend to have stronger nuclear starbursts than do Seyfert 1 galaxies. As the $L_{3.3PAH}$ of Seyfert 1 and 2 galaxies do not differ significantly, we have interpreted this as the result of the effect that the AGN emission of Seyfert 2s is absorbed by dust of torus and then the stellar emission becomes relatively larger.
2. The $L_{3.3PAH}$ shows the same range in Seyfert 1 and 2 galaxies. The star-formation rates of our sample are up to 4.5–450 $\times 10^{-3} \mathrm{M}_{\odot}$ yr^{-1}, which could be enough to swell the dusty torus by supernova explosion; in short, it is geometrically thick, although many objects we provided are only with upper limits on the 3.3 μm PAH luminosities.
3. The $L_{3.3PAH}$ correlates with mid-infrared (N-band) luminosity with small aperture (= tracing AGN activities), and their luminosity ratio does not vary significantly over a wide AGN luminosity range. Moreover the $L_{3.3PAH}$ is independent of physical scale we probed with slits. Therefore the $L_{3.3PAH}$ (i.e. star formation) would concentrate on the central region, and the nuclear star formation would induce the accretion onto the SMBH and encourage the AGN activity. In this work, we find no evidence that nuclear starbursts are stronger in lower-luminosity AGN.
4. We suggest that the 3.3 μm PAH emission luminosity and K-band stellar luminosity ($L_{Kstellar}$) originate in the same phenomenon. However, for some fraction of Seyfert 2 galaxies, $L_{Kstellar}$ is likely to be overestimated because of flux attenuation of AGN emission caused by a dusty torus and contaminated by old stars in the spheroid of the host galaxy.

acknowledgments

We would like to thank the staff at the IRTF 3.0-m telescope for their help with observations. We thank C. Packham, N. Kawakatu, H. Ando, N. Arimoto, and T. Kodama for useful discussions. M.I. was supported by grants-in-aid for scientific research (19740109). This work was supported in part by The Graduate University for Advanced Studies (Sokendai). This research made use of the NASA/IPAC Extragalactic Database (NED), which is operated by the Jet Propulsion Laboratory, California Institute of Technology, and the SIMBAD database, operated at CDS, Strasbourg, France.

References

Alonso-Herrero, A., Ward, M. J., & Kotilainen, J. K. 1996, MNRAS, 278, 902

Alonso-Herrero, A., Ivanov, V. D., Jayawardhana, R., & Hosokawa, T. 2002, ApJ, 571, L1

Alonso-Herrero, A., Quillen, A. C., Rieke, G. H., Ivanov, V. D., & Efstathiou, A. 2003, ApJ, 126, 81

Antonucci, R. 1993, ARA&A, 31, 473

Ballantyne, D. R., 2008, ApJ, 685, 787

Ballo, L., Braito, V., Della Ceca, R., Maraschi, L., Tavecchio, F., & Dadina, M. 2004, ApJ, 600, 634

Braito, V., et al. 2004, A&A, 420, 79

Davies, R. I., Sánchez, F. M., Genzel, R., Tacconi, L. J., Hicks, E. K. S., Friedrich, S., & Sternberg, A. 2007, ApJ, 671, 1388

Della Ceca, R., et al. 2002, ApJL, 581, L9

Doyon, R., Joseph, R. D., & Wright, G. S. 1994, ApJ, 421, 101

Frogel, J. A., Persson, S. E., Matthews, K., & Aaronson, M. 1978, ApJ, 220, 75

Galliano, E., Alloin, D., Pantin, E., Lagage, P. O., & Marco, O. 2005, A&A, 438, 803

Goldader, J. D., Joseph, R. D., Doyon, R., & Sanders, D. B. 1997, ApJ, 474, 104

Gorjian, V., Werner, M. W., Jarrett, T. H., Cole, D. M., & Ressler, M. E. 2004, ApJ, 605, 156

Haas, M., Siebenmorgen, R., Schulz, B., Krugel, E., & Chini, R. 2005, A&A, 442, L39

Ho, L. C., Filippenko, A. V., & Sargent, W. L. W. 1995, ApJS, 98, 477

Ho, L. C., Filippenko, A. V., & Sargent, W. L. W. 1997, ApJ, 487, 568

Ho, L. C., & Ulvestad, J. S. 2001, ApJS, 133, 77

Horst, H., Duschl, W. J., Gandhi, P., & Smette, A. 2009, A&A, 495, 137

Huchra, J., & Burg, R. 1992, ApJ, 393, 90

Imanishi, M. 2003, ApJ, 599, 918

Imanishi, M., Terashima, Y., Anabuki, N., & Nakagawa, T. 2003, ApJL, 596, L167

Imanishi, M., & Alonso-Herrero, A. 2004, ApJ, 614, 122

Imanishi, M., & Dudley, C. C. 2000, ApJ, 545, 701

Imanishi, M., Dudley, C. C., & Maloney, P. R. 2001, ApJL, 558, L93

Imanishi, M., & Nakanishi, K. 2006, PASJ, 58, 813

Imanishi, M., & Wada, K. 2004, ApJ, 617, 214

Isobe, T., Feigelson, E. D., & Nelson, P. I. 1986, ApJ, 306, 490

Ivanov, V. D., Rieke, G. H., Groppi, C. E., Alonso-Herrero, A., Rieke, M. J., & Engelbracht, C. W. 2000, ApJ, 545, 190

Kawakatu, N. & Wada, K. 2008, ApJ, 681, 73

Kennicutt, R. C., Jr, 1998, ApJ, 498, 541

Kotilainen, J. K., Ward, M. J., Boisson, C., Depoy, D. L., & Smith, M. G. 1992, MNRAS, 256, 149

Levenson, N. A., Radomski, J. T., Packham, C., Mason, R. E., Schaefer, J. J., & Telesco, C. M. 2009, ApJ, 703, 390 isher, R. S., & Perlman, E. 2006, ApJ, 640, 612

Mouri, H., Kawara, K., Taniguchi, Y., & Nishida, M. 1990, ApJ, 356, 39

Moorwood, A. F. M. 1986, A&A, 166, 4

Nishiyama, S., Nagata, T., Tamura, M., Kandori, R., Hatano, H., Sato, S., & Sugitani, K. 2008, ApJ, 680, 1174

Nishiyama, S., Tamura, M., Hatano, H., Kato, D., Tanabe, T., Sugitani, K., & Nagata, T. 2009, ApJ, 696, 1407

Oliva, E., Origlia, L., Maiolino, R., & Moorwood A.F.M. 1999, A&A 350, 9

Osterbrock, D. E., & Martel, A. 1993, ApJ, 414, 552

Ramos Almeida, C., et al. 2009, ApJ, 702, 1127

Rayner, J. T., Toomey, D. W., Onaka, P. M., Denault, A. J., Stahlberger, W. E., Vacca, W. D., Cushing, M. C., & Wang, S. 2003, PASP, 115, 362

Ridgway, S. E., Wynn-Williams, C. G., & Becklin, E. E. 1994, ApJ, 428, 609

Rodríguez-Ardila, A., & Viegas, S. M. 2003, MNRAS, 340, L33

Rodriguez Espinosa, J. M., & Perez Garcia, A. M. 1997, ApJL, 487, L33

Rush, B., Malkan, M. A., & Spinoglio, L. 1993, ApJS, 89, 1

Sanders, D. B., & Mirabel, I. F. 1996, ARA&A, 34, 749

Sellgren, K. 1981, ApJ, 245, 138

Spinoglio, L., & Malkan, M. A. 1989, ApJ, 342, 83

Tanaka, M., Matsumoto, T., Murakami, H., Kawada, M., Noda, M., & Matsuura, S. 1996, PASJ, 48, L53

Tokunaga, A. T., Sellgren, K., Smith, R. G., Nagata, T., Sakata, A., & Nakada, Y. 1991, ApJ, 380, 452

Tokunaga, A. T. 2000, in Allen's Astrophysical Quantities, 4th ed. Arthur N. Cox., 143

Voit, G. M. 1992, MNRAS, 258, 841

Wada, K., & Norman, C. A. 2002, ApJ, 566, L21

Wada, K., Papadopoulos, P., Spaans, M., 2009, ApJ, 702, 63

Willner, S. P., Fabbiano, G., Elvis, M., Ward, M., Longmore, A., & Lawrence, A. 1984, PASP, 96, 143

Zezas, A., Ward, M. J., & Murray, S. S. 2003, ApJL, 594, L31

Table 1. Target information

Object (1)	z (2)	D_L (3)	Class (4)	f_{12} (5)	f_{25} (6)	f_{60} (7)	f_{100} (8)	$f_{10.8}$ (9)	$logL_{IR}$ (10)
Palomar sample									
NGC676	0.0050	20.2	Sy2	0.04	0.06	0.27	0.80	...	42.3
NGC1167	0.0165	66.8	Sy2	<0.03	<0.04	0.12	1.05	...	43.3
NGC1275	0.0176	71.2	Sy1	0.93	3.02	7.09	7.60	...	44.8
NGC1358	0.0134	54.3	Sy2	<0.08	<0.12	0.38	0.93	...	43.4
NGC3982[b,c]	0.0035	14.2	Sy2	0.47	0.97	7.18	16.20	<0.1 1	43.3
NGC4258[b]	0.0015	6.2	Sy2	2.25	2.81	2.81	78.40	...	43.0
NGC4579[b,c]	0.0050	20.3	Sy2	1.12	0.78	5.93	21.40	0.08(0. 06*)	43.7
NGC5194[b,c]	0.0020	8.0	Sy2	7.21	9.56	97.40	221.00	<0.0 7	43.9
NGC5273[b]	0.0036	14.4	Sy1	0.12	0.29	0.90	1.560	...	42.5
NGC6764	0.0080	32.4	Sy2	0.54	1.33	6.62	12.40	...	44.0
NGC6951	0.0048	19.1	Sy2	1.34	2.16	16.20	41.80	...	44.0
NGC7479[b]	0.0079	32.0	Sy2	1.37	3.86	14.90	26.70	...	44.4
NGC7743[b]	0.0057	22.9	Sy2	0.10	0.18	0.92	3.40	...	43.0
CfA & 12 μm									
NGC262[c]	0.0151	61.3	Sy2	0.31	0.84	1.29	1.55	0 .12	44.0
NGC513[c]	0.0195	79.4	Sy2	0.17	0.28	1.94	4.05	<0 .10	44.2
NGC931[c]	0.0167	67.5	Sy1	0.61	0.61	1.32	4.55	0 .21	44.3
NGC5548[a,b,c]	0.0172	67.6	Sy1	0.40	0.77	1.07	1.61	0 .29	44.1
Mrk993[b,c]	0.0155	62.8	Sy1	<0.13	<0.13	0.30	1.32	...	43.6
MCG-2-8-39[c]	0.0299	122.3	Sy2	0.20	0.48	0.51	<1.42	...	44.4
MCG-3-58-7[c]	0.0320	131.1	Sy2	0.28	0.80	2.42	3.36	0 .20	44.8
F03450+0055[c]	0.0310	126.9	Sy1	0.28	0.51	0.47	<3.24	0 .10	44.6
0152+06[b]	0.0174	70.6	Sy2	<0.08	<0.16	0.50	1.15	...	43.7

Col.(1): object name. a, b, c are reference; a)Palomar sample (Ho & Ulvestad 2001), b)CfA (Huchra & Burg 1992), c)12 μm (Rush et al. 1993). Col.(2): redshift. Col.(3): luminosity distance in Mpc. Col.(4): AGN class. Col.(5)-(8): flux at 12μm, 25μm, 60μm, and 100μm in Jy, respectively from $IRAS$ faint source catalog. Col.(9): ground-based 10.8μm photometric data, observed with the Palomar 5-m telescope using a $1\farcs5$ aperture (Gorjian et al. 2004). NGC4579 was observed also by Horst et al. (2009) using VLT/VISIR with a $1\farcs27$ small aperture. Col.(10): decimal logarithm of infrared (8-1000μm) luminosity in ergs s^{-1} calculated with $L_{IR} \equiv 2.17 \times 10^{39} \times D_L(\mathrm{Mpc})^2 \times$(13.48$\times f_{12}$+5.16$\times f_{25}$+2.58$\times f_{60}$+$f_{100}$) ergs s^{-1} (Sanders & Mirabel 1996).

Table 2. Observing Log

Object (1)	Date (2)	Itime (3)	Slit (4)	Std star (5)	Type (6)	V (7)	K (8)	L (9)	T_{eff} (10)
Palomar sample									
NGC676	2009 Oct. 27	48	0.8	HD13043	G2V	6.87	5.39	5.34	5830
NGC1167	2009 Oct. 26	70	1.6	HD19600	A0V	6.42	6.32	6.32	9480
NGC1275	2009 Oct. 27	44	0.8	HD20995	A0V	5.61	5.61	5.61	9480
NGC1358	2009 Oct. 28	120	0.8	HD21019	G2V	6.20	4.42	4.37	5830
NGC3982	2005 Apr. 29	68	0.8	HR4496	G8V	5.33	3.53	3.47	5430
NGC4258	2005 Apr. 27	80	0.8	HR4572	F6V	6.62	5.41	5.37	6385
NGC4579	2005 Apr. 28	40	0.8	HR4708	F8V	6.40	5.05	5.01	6130
NGC5194	2005 May. 1	60	0.8	HR4845	G0V	5.95	4.54	4.49	5930
NGC5273	2005 Apr. 29	60	0.8	HR4845	G0V	5.95	4.54	4.49	5930
NGC6764	2005 May. 1	60	0.8	HR7294	G4V	6.57	5.04	4.99	5740
NGC6951	2005 Apr. 30	100	0.8	HR7783	G3V	5.93	4.44	4.39	5785
NGC7479	2009 Oct. 26	56	0.8	HD217577	G2V	8.66	7.12	7.07	5830
NGC7743	2009 Oct. 27	75	1.6	HD377	G2V	7.60	6.12	6.07	5830
CfA & 12 μm									
NGC262	2007 Aug. 31	80	0.8	HR410	F7V	6.31	4.99	4.95	6240
NGC513	2007 Aug. 27	120	0.8	HR410	F7V	6.31	4.99	4.95	6240
NGC931	2007 Aug. 26	96	0.8	HR720	G0V	5.89	4.48	4.43	5930
NGC5548	2005 Apr. 29	20	0.8	HR5346	F8V	6.25	4.90	4.85	6130
Mrk993	2007 Aug. 31	112	0.8	HR410	F7V	6.31	4.99	4.95	6240
MCG-2-8-39	2007 Aug. 30	136	0.8	HR784	F6V	5.78	4.57	4.53	6385
MCG-3-58-7	2007 Aug. 30	80	0.8	HR8457	F6V	6.09	4.88	4.84	6385
F03450+0055	2007 Aug. 28	112	0.8	HR962	F8V	5.06	3.71	3.67	6130
				HR145	F7V	6.41	5.09	5.05	6240
0152+06	2007 Aug. 29	120	0.8	HR508	G3Va	6.27	4.78	4.73	5785

Col.(1): object name. Col.(2): observing date in UT. Col.(3): net on-source exposure time in minutes. Col.(4): slit width in arcsec. Col.(5): name of standard stars. HR962 was observed as the standard star for F03450+0055. However, because it was saturated in some part of the K-band spectrum, we used HR145, which was observed on the same day, as the K-band standard star for F03450+0055. Col.(6): stellar spectral type. Col.(7)-(9): V, K and L-band magnitude. Col.(10): effective temperature in K.

Table 3. Properties of the nuclear 3.3 μm PAH emission and CO absorption feature s

Object	$f_{3.3PAH}$ ($\times 10^{14}$ergs s^{-1}cm^{-2})	$log(L_{3.3PAH})$ (ergs s^{-1})	$EW_{3.3PAH}$ (nm)	CO_{spec}	$K-L$ (mag)	SFR (M$_\odot$ yr^{-1})
(1)	(2)	(3)	(4)	(5)	(6)	(7)
Palomar sample						
NGC676	<11.58	<39.73	<10.79	0.20	−0.08	<0.24
NGC1167	< 7.85	<40.60	<18.02	0.23	0.14	<1.80
NGC1275	<31.58	<41.26	< 4.26	0	1.79	<8.22
NGC1358	< 9.21	<40.49	<21.53	0.18	−0.04	<1.39
NGC3982	< 6.17	<39.15	<28.42	0.16	0.27	<0.06
NGC4258	<13.57	<38.77	< 4.17	0.16	0.95	<0.03
NGC4579	< 3.22	<39.17	< 1.37	0.18	0.61	<0.07
NGC5194	6.99	38.71	12.08	0.20	0.14	0.02
NGC5273	8.55	39.30	9.57	0.11	0.72	0.09
NGC6764	40.50	40.68	91.72	0.22	0.54	2.18
NGC6951	< 6.05	<39.40	<19.64	0.24	0.15	<0.11
NGC7479	<16.53	<40.28	<10.77	0.10	1.59	<0.87
NGC7743	< 4.39	<39.42	< 4.76	0.25	0.28	<0.12
CfA & 12 μm						
NGC262	<13.01	<40.74	< 1.94	0.02	1.98	<2.51
NGC513	< 4.35	<40.49	< 5.92	0.11	1.11	<1.41
NGC931	<11.15	<40.76	< 1.34	0	1.74	<2.61
NGC5548	<14.63	<40.88	< 5.09	0.01	1.54	<3.43
Mrk993	< 4.72	<40.32	<10.98	0.16	0.57	<0.96
MCG-2-8-39	< 6.24	<41.02	<21.46	0.16	1.20	<4.80
MCG-3-58-7	10.64	41.32	1.96	0.02	1.84	9.40
F03450+0055	3.36	40.79	0.56	0.01	1.65	2.78
0152+06	< 2.35	<40.12	< 6.70	0	1.02	<0.60

Col.(1): object name. Col.(2): nuclear 3.3μm PAH emission flux in 10^{-14}ergs s^{-1}cm^{-2}. Col.(3): decimal logarithm of nuclear 3.3μm PAH emission luminosity in ergs s^{-1}. Col.(4): rest-frame equivalent width of 3.3μm PAH emission line in nm. Col.(5): spectroscopic CO_{spec} index at λ_{rest}=2.3-2.4 μm in the rest frame. The definition appears in the text §4.2. Col.(6): $K-L$ color (mag) measured in this work. K- and L-band magnitudes were derived by integrating the flux from 1.97–2.38μm and 3.26–3.83μm, respectively. Col.(7): nuclear star-formation rate in $\mathrm{M}_\odot\ yr^{-1}$ inside our slit sizes.

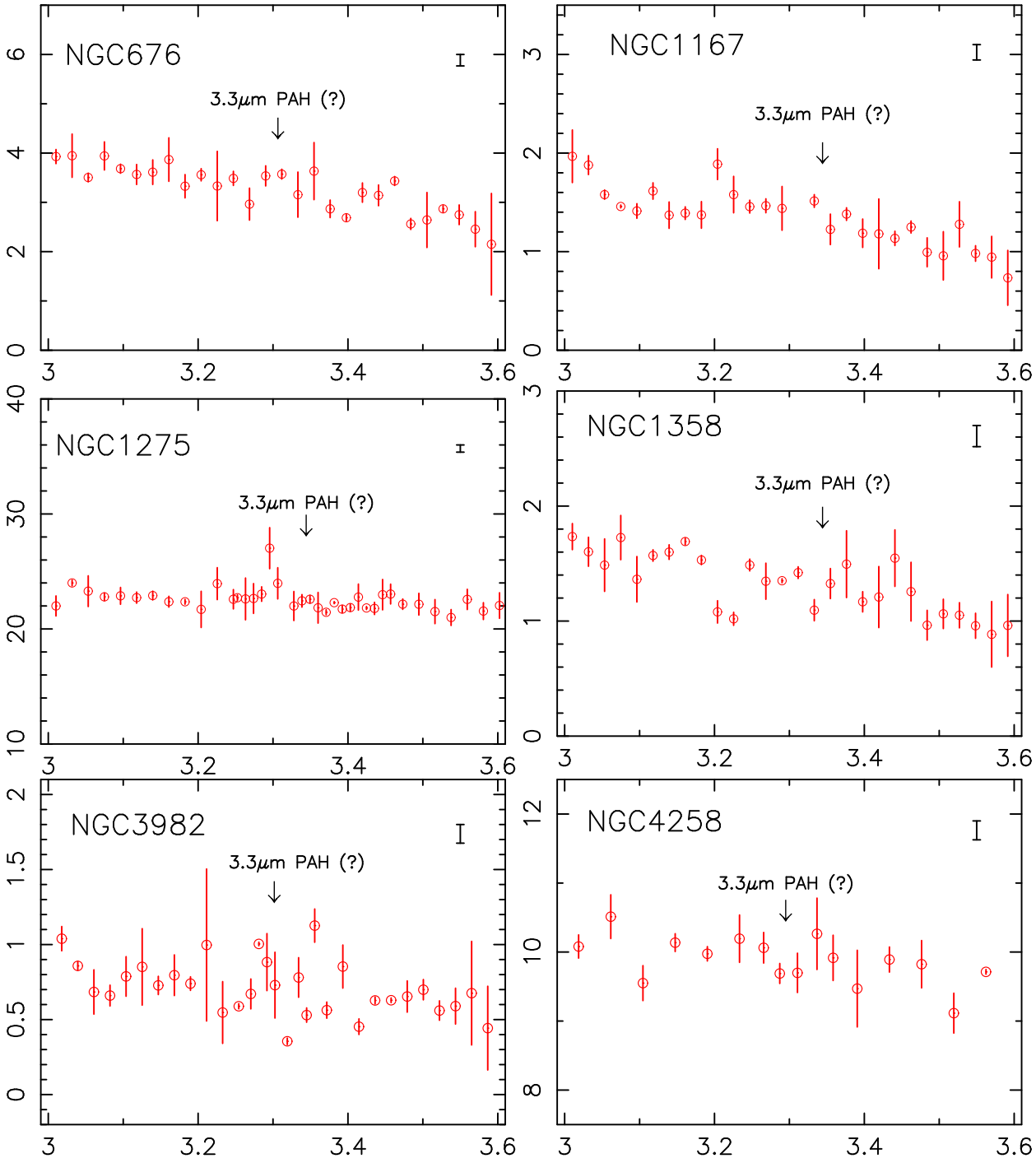

Fig. 1. Infrared 3.0-3.6μm slit spectra (L-band) of 22 Seyfert nuclei. The abscissa and ordinate are the observed wavelength in μm and F_λ in $10^{-15}\mathrm{Wm}^{-2}\mu\mathrm{m}^{-1}$, respectively. The length of the bar at the upper right of each figure indicates the 1σ error for the continuum. The phrase "3.3 μm PAH" ("3.3 μm PAH(?)") indicates the detectable (undetectable) 3.3 μm PAH emission. The best-fit Gaussian profile is shown for objects with detected 3.3 μm PAH emission. For our 3.3 μm PAH detection criteria, please refer to §4.1 in the text.

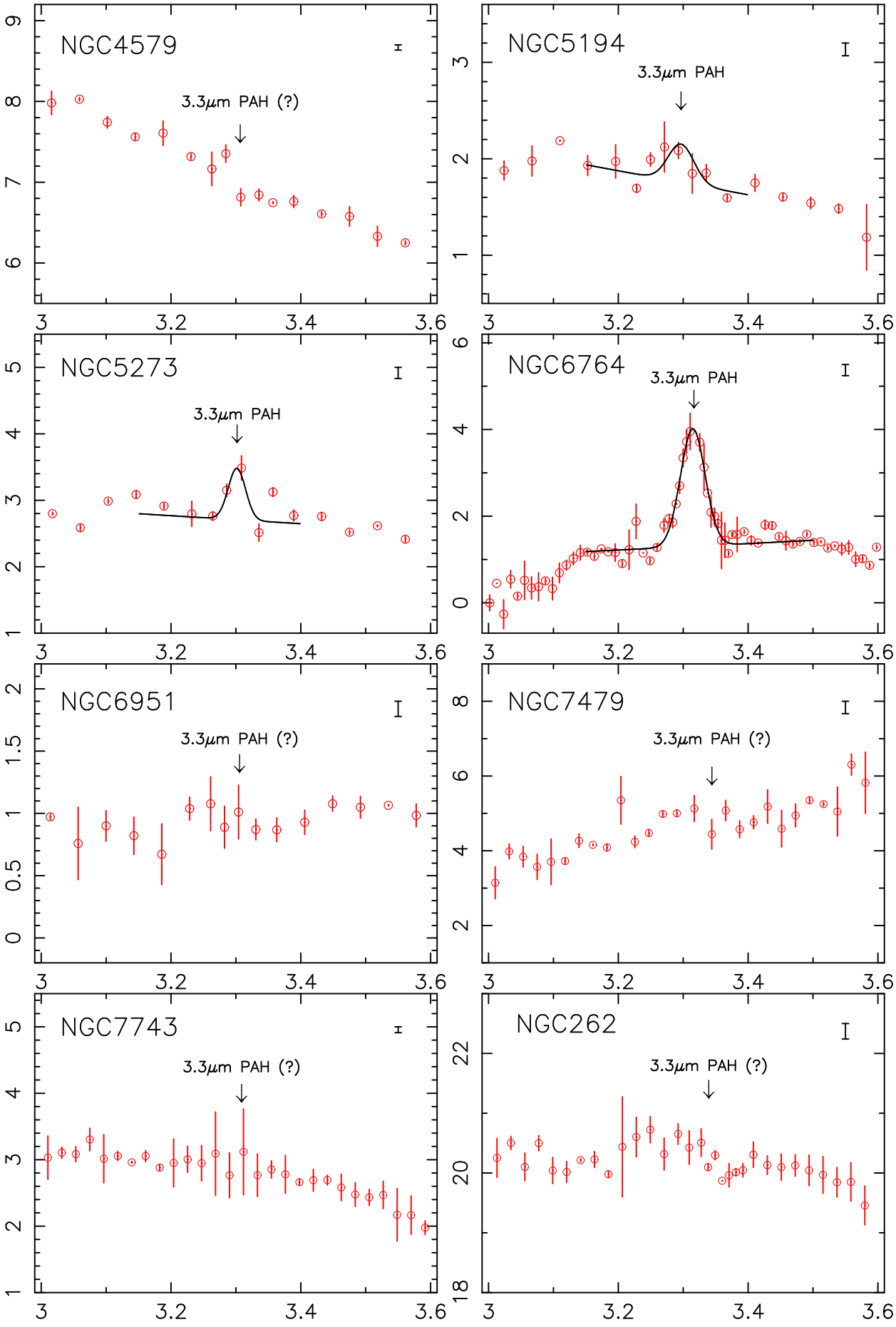

Fig. 1. –Continued

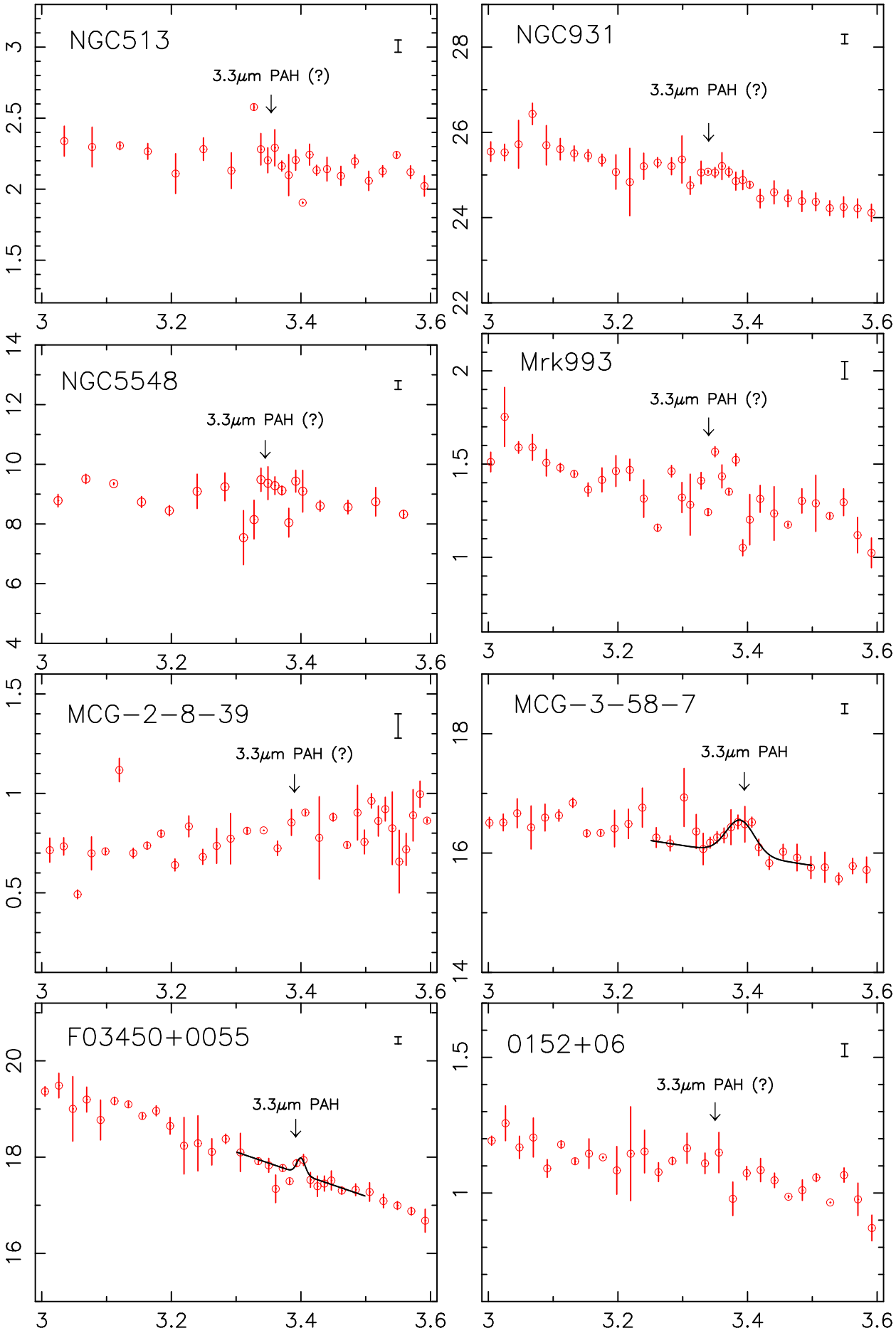

Fig. 1. –Continued

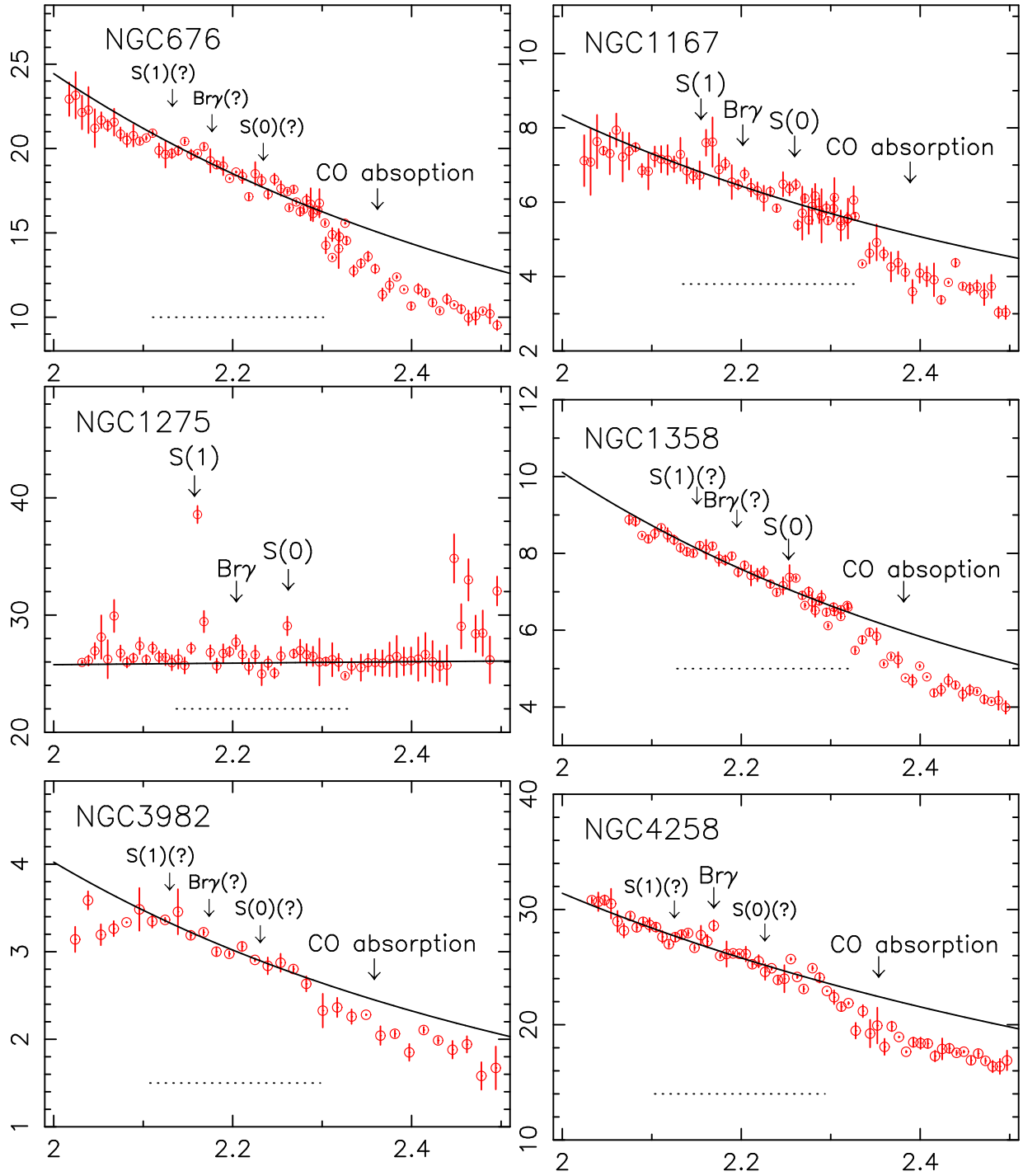

Fig. 2. Infrared 2.0-2.5μm slit spectra (K-band) of 22 Seyfert nuclei. The abscissa and ordinate are the same as in Figure 1. The phrases "S(1)", "Brγ", and "S(0)" show the excess emission lines of H_2 1-0 S(1) ($\lambda_{rest} = 2.122\mu$m), Br$\gamma$ ($\lambda_{rest} = 2.166\mu$m) and H_2 1-0 S(0) ($\lambda_{rest} = 2.223\mu$m), respectively. Indistinct lines are marked as "S(1)(?)", "Brγ(?)", and "S(0)(?)". The symbol "CO absorption" indicates a clear absorption feature at $\lambda_{rest} = 2.3 - 2.4\mu$m.

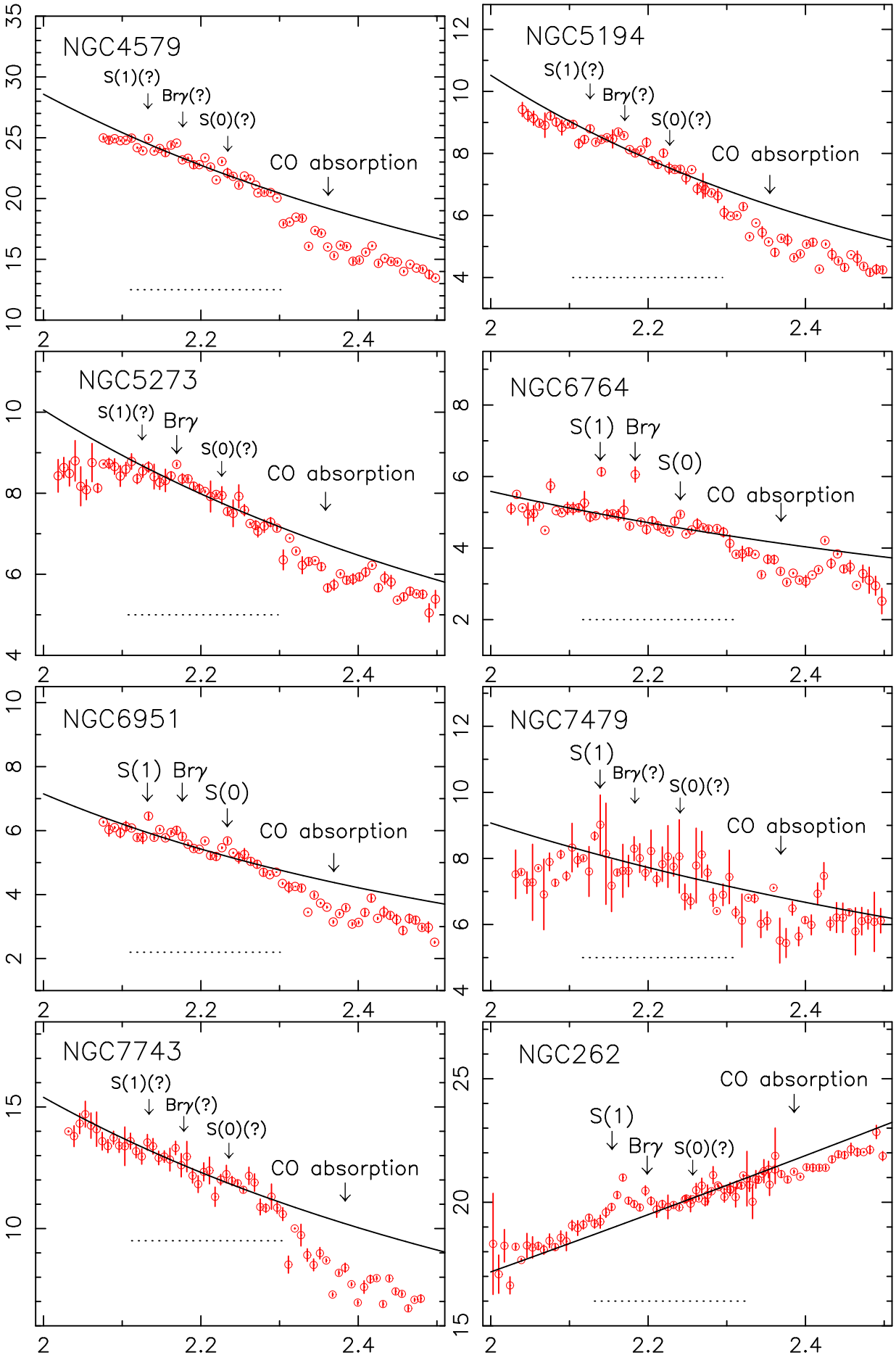

Fig. 2. –Continued

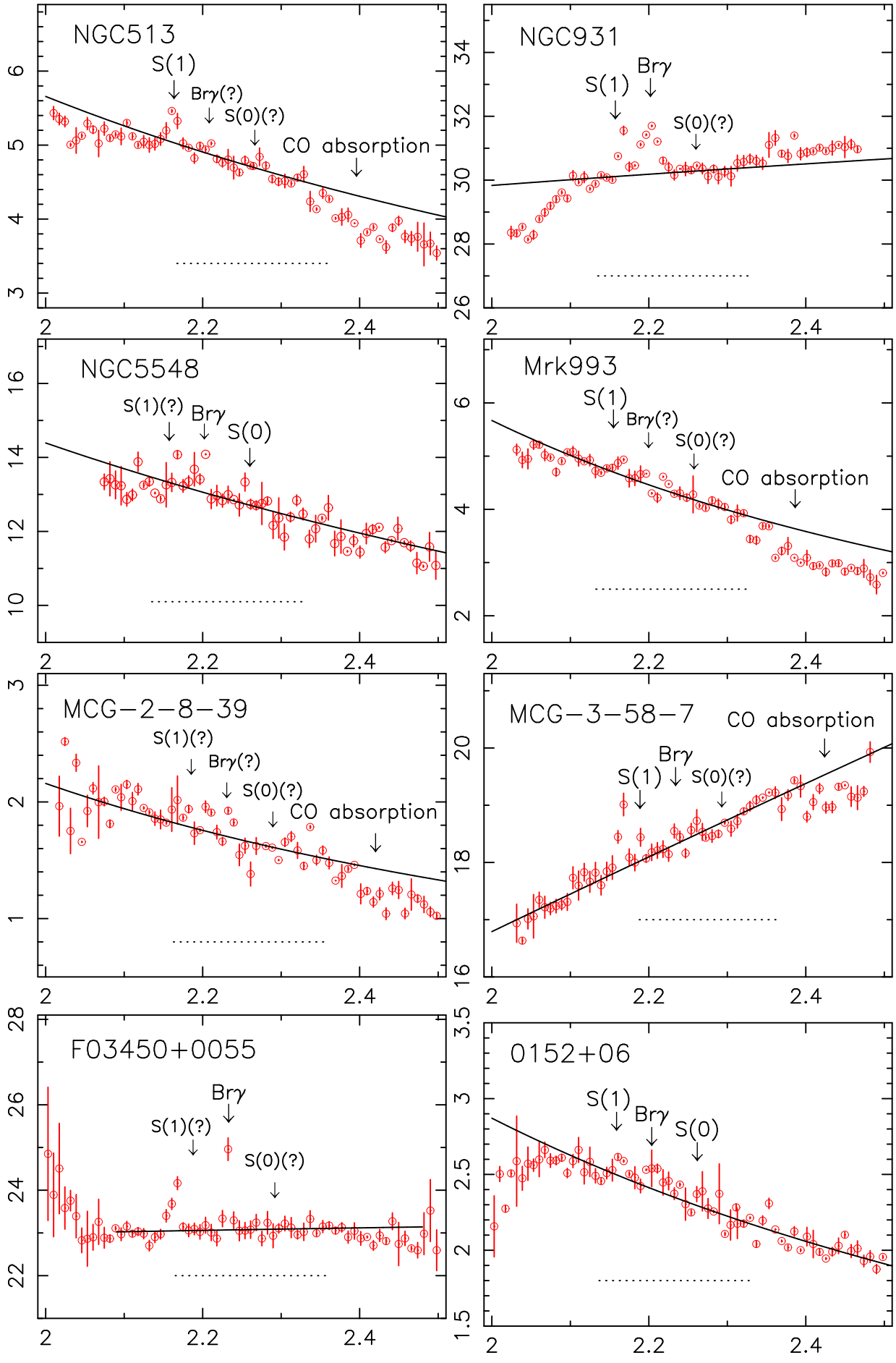

Fig. 2. –Continued

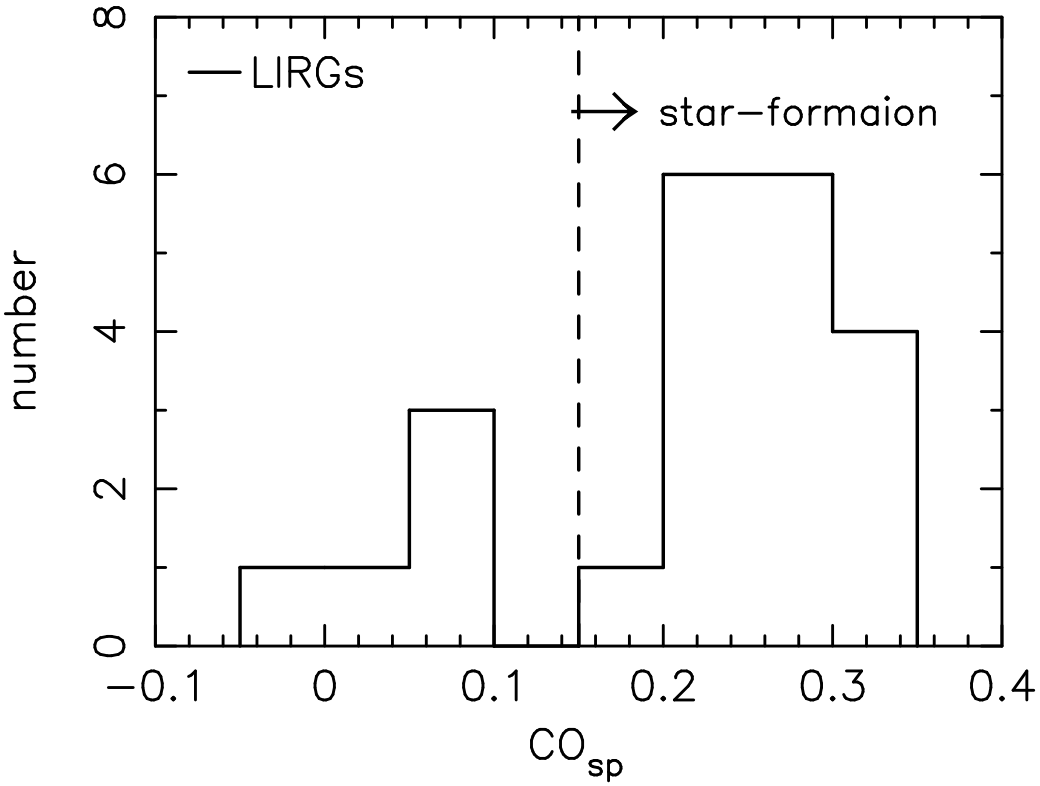

Fig. 3. Histogram of the CO_{spec} index of LIRGs (Ridgway et al. 1994). The five objects with CO_{spec} smaller than 0.1 (Mrk231, IRAS05189-2524, UCG5101, Arp299B1, and Arp299C) showed strong AGN signs in previous studies (Imanishi & Dudley 2000; Imanishi et al. 2001; Della Ceca et al. 2002; Zezas et al. 2003; Imanishi et al. 2003; Ballo et al. 2004; Braito et al. 2004; Imanishi & Nakanishi 2006).

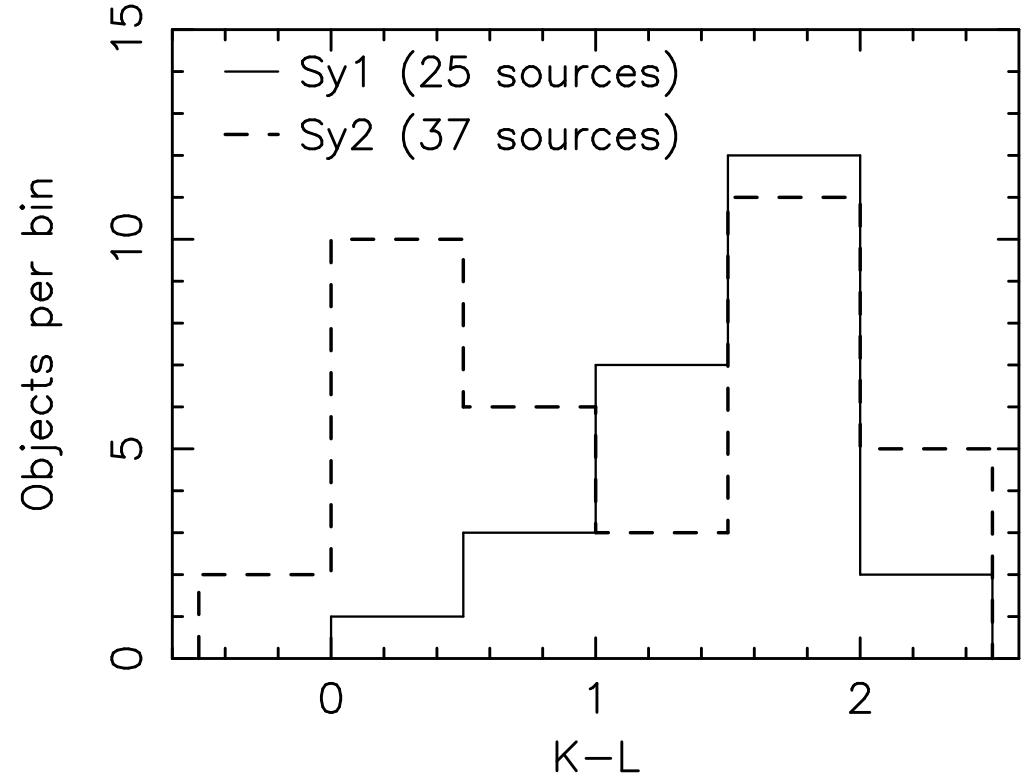

Fig. 4. Histogram of the $K-L$ color of Seyfert galaxies. In addition to the objects studied in this paper, data from Imanishi & Alonso-Herrero (2004) and Imanishi & Wada (2004) are included. The solid line represents Seyfert 1 galaxies, and the dashed line represents Seyfert 2 galaxies.

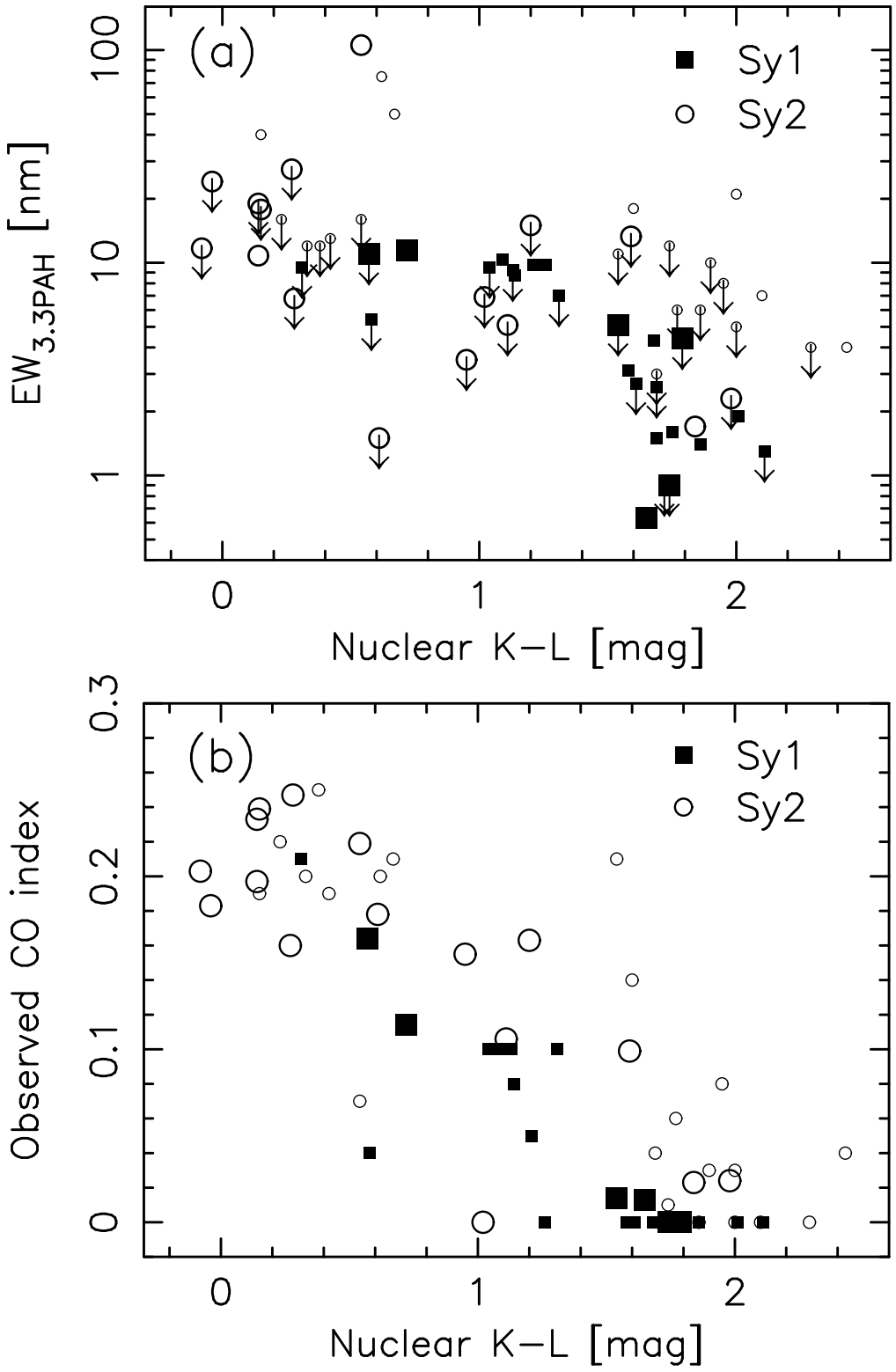

Fig. 5. (a):Comparison of the $K-L$ color (abscissa) and equivalent width of the 3.3 μm PAH emission detected inside our slit spectra (ordinate). (b):The ordinate is the observed CO_{spec} index. Filled squares represent the data for Seyfert 1 galaxies, and open circles for Seyfert 2 galaxies. Large symbols represent our sample, and small symbols represent previously gathered data (Imanishi & Alonso-Herrero 2004; Imanishi & Wada 2004).

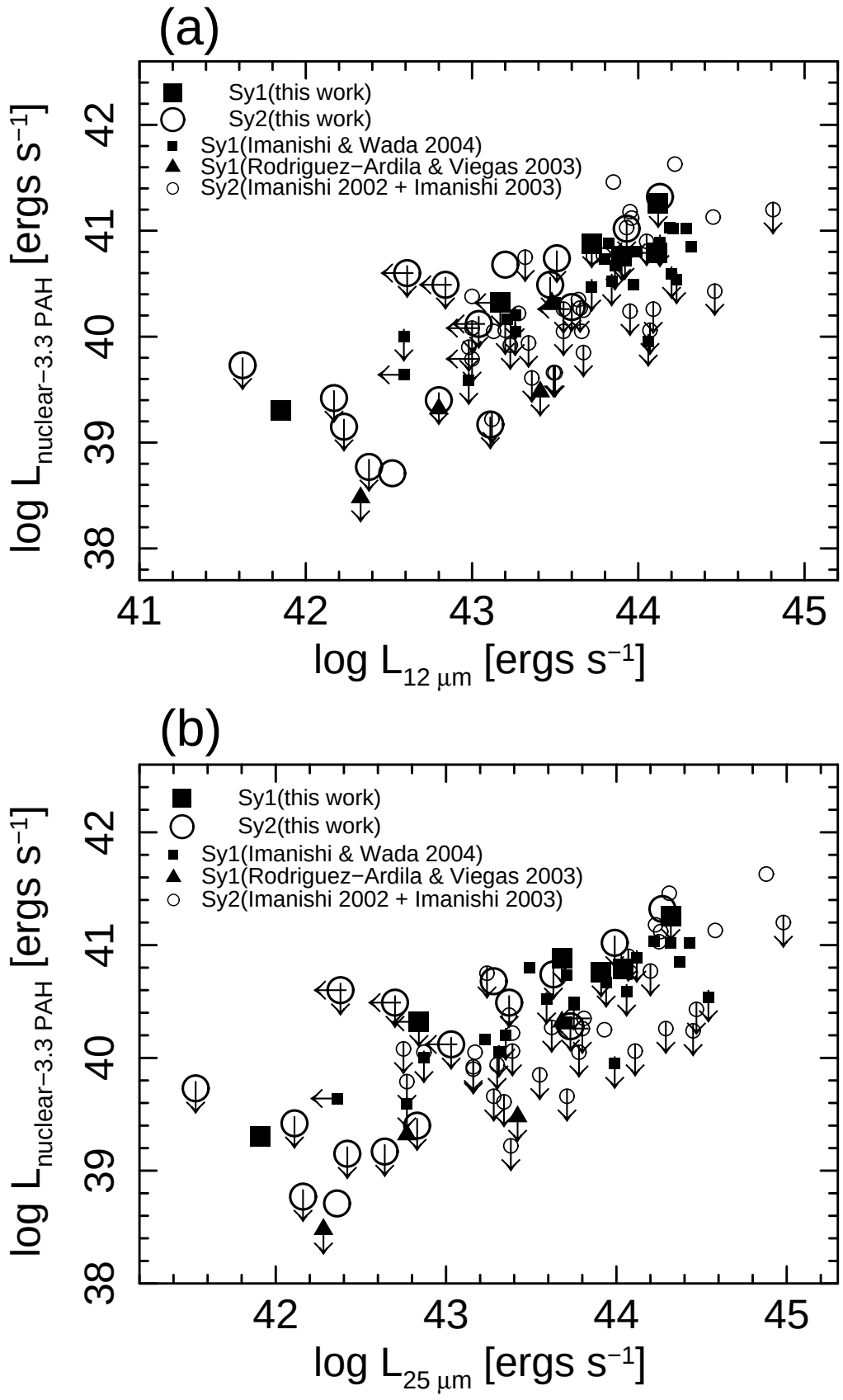

Fig. 6. (a): $IRAS$ 12 μm luminosity, defined as νL_ν (abscissa) versus the 3.3 μm PAH emission luminosity detected inside our slit spectra (ordinate). Indices are the same as in Fig. 5. Seyfert 1 galaxies studied by other groups (IH1934-063, Mrk766, NGC3227, and NGC4051; Rodríguez-Ardila & Viegas 2003) are plotted as filled triangles. (b): Same as (a), but the abscissa is $IRAS$ 25 μm luminosity.

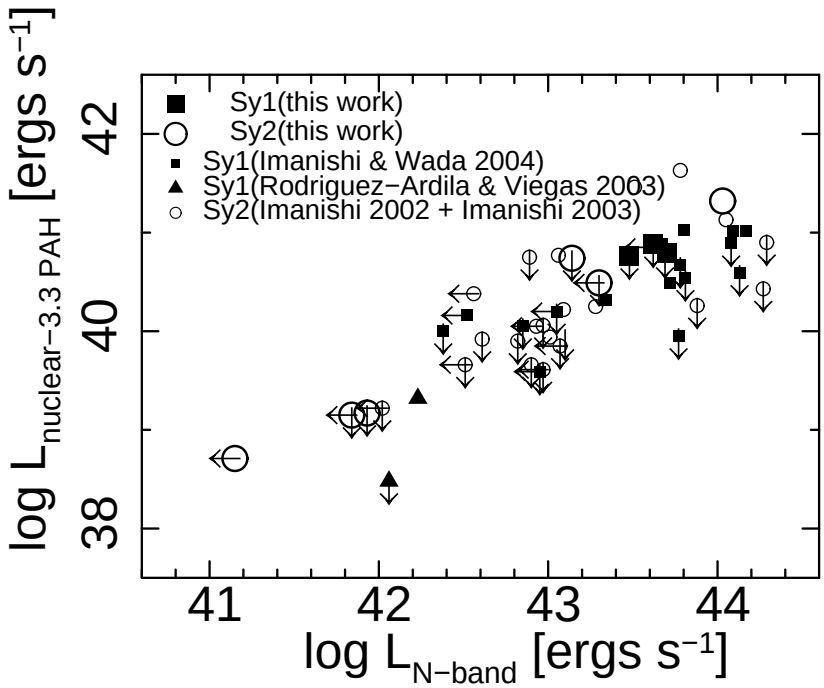

Fig. 7. Same as Fig. 6, but the abscissa is ground-based N-band luminosity measured with small aperture. Almost all N-band data in the abscissa are 10.8 μm luminosity measured with a 1.″5 aperture (Gorjian et al. 2004). Galliano et al. (2005) observed 10.4 μm luminosity with 2-arcsec aperture for NGC2992 and NGC7469 using ESO 3.6-m telescope/TIMMI2, and Horst et al. (2009) observed 10.49 μm luminosity with 1.27-arcsec aperture for NGC4579, Mrk509 and MCG -3-34-64 using VLT/VISIR. We adopted the new values for the five objects. Among the four sources studied by Rodríguez-Ardila & Viegas (2003), only two objects (NGC3227 and NGC4051) are plotted because of the availability of measured 10.8 μm luminosity (Gorjian et al. 2004). The abscissa is a good indicator of AGN power, and the ordinate probes nuclear starburst luminosities.

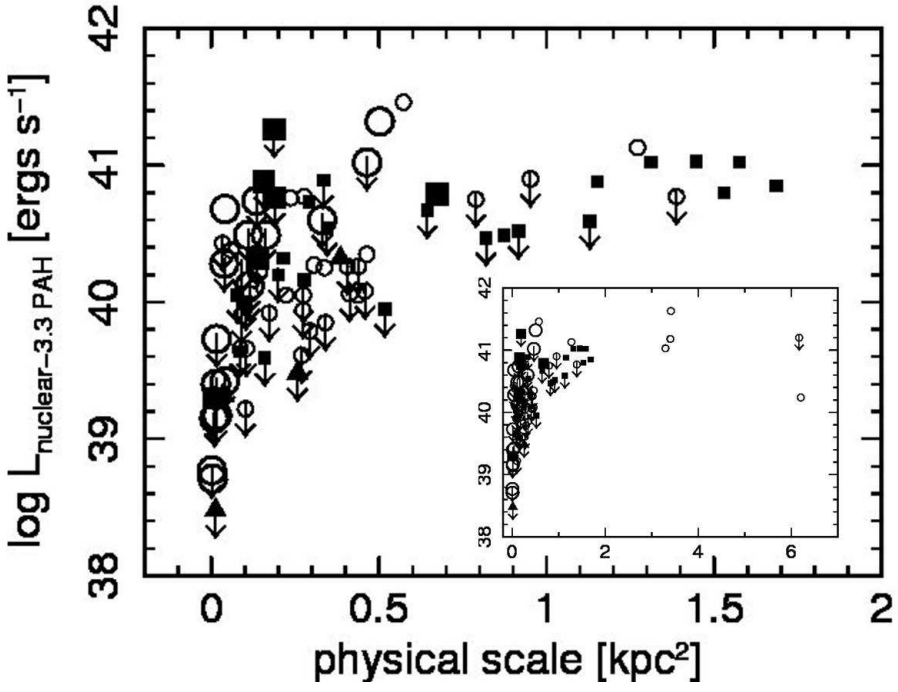

Fig. 8. Relationship between physical scale we probed with slits and the 3.3 μm PAH emission luminosity inside the slits (same symbols as in Figure 6). Since all physical areas of objects except 5 objects (Mrk34, Mrk78, Mrk273, Mrk463, Mrk477) plotted in the figure are smaller than 2 square kpc, larger figure focus on the physical area from 0.001 to 1.827 kpc^2 to show the distribution. A figure including these 5 objects are pasted small on the lower right of larger figure.

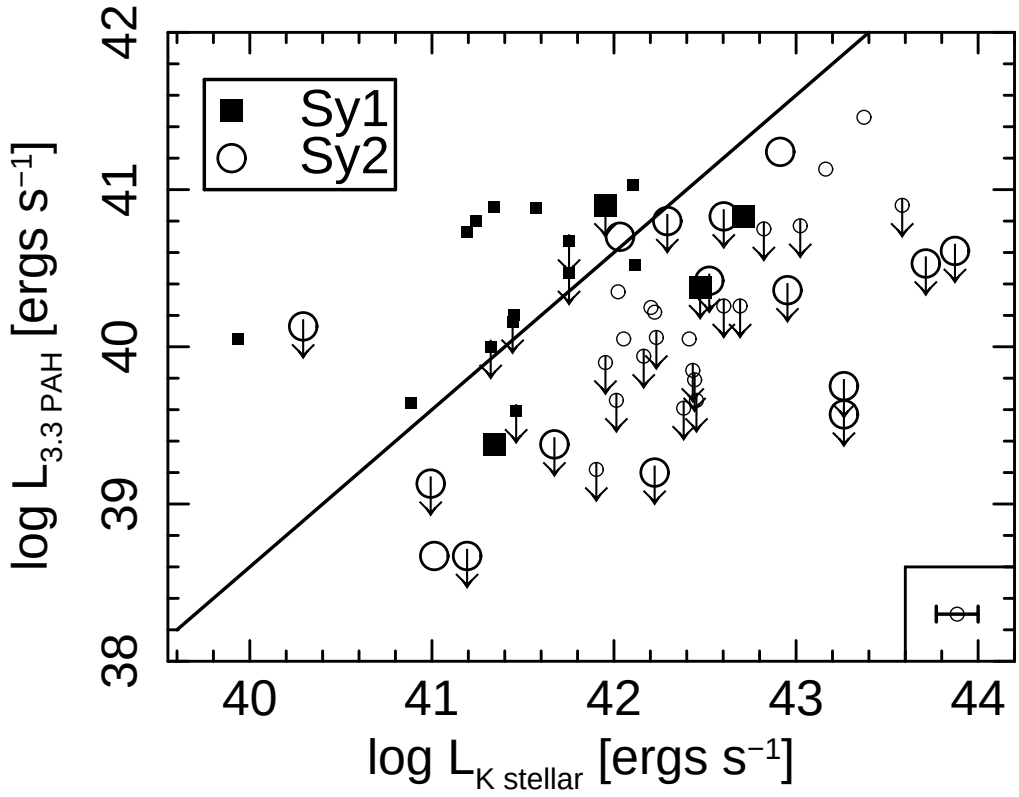

Fig. 9. Comparison between the K-band stellar luminosity (abscissa) and the nuclear 3.3 μm PAH luminosity detected inside our slit spectra (ordinate). Symbols are the same as in Figure 5. The length of the bar at the lower right of the figure represents the range in uncertainty of $L_{Kstellar}$ due to $CO_{spec} = 0.2 - 0.3$. The solid line shows the predicted ratio of $L_{3.3PAH}/L_{Kstellar}$ ($\sim 10^{-1.4}$) for starbursts as seen in LIRGs.